

## Calcium Adsorption on MgO(100): Energetics, Structure, and Role of Defects

Junfa Zhu,<sup>†</sup> Jason A. Farmer,<sup>†</sup> Nancy Ruzycki,<sup>†</sup> Lijun Xu,<sup>‡</sup>  
Charles T. Campbell,<sup>\*,†</sup> and Graeme Henkelman<sup>\*,‡</sup>

*Department of Chemistry, University of Washington, Seattle, Washington 98195-1700,  
Department of Chemistry and Biochemistry, University of Texas, Austin, Texas 78712-0165*

Received October 13, 2007; E-mail: campbell@chem.washington.edu; henkelman@mail.utexas.edu

**Abstract:** The adsorption of Ca on the MgO(100) surface at 300 K has been studied using microcalorimetry, in combination with LEED, AES, ISS, work function, sticking probability measurements, and density functional theory (DFT) calculations. The MgO(100) thin films (~4 nm thick) were grown epitaxially on a 1  $\mu\text{m}$  thick Mo(100) single-crystal. The sticking probability of Ca on MgO(100) at 300 K is unity. On the basis of AES and ISS measurements, it was determined that Ca grows mainly as 3D particles on the MgO(100) surface with a density of  $\sim 1 \times 10^{12}$  islands/cm<sup>2</sup>. Ca adsorbs initially at defect sites with a very high heat of adsorption ( $\sim 410$  kJ/mol). DFT calculations attribute this high initial heat to Ca binding to kink sites (376 kJ/mol), step sites (205 kJ/mol), and lower concentrations of stronger binding sites. The heat of adsorption decreases rapidly with coverage, reaching a minimum of 162 kJ/mol at  $\sim 0.3$  ML, where Ca is mainly adding to small 3D Ca clusters. Afterward, it increases to the value of bulk Ca heat of sublimation (178 kJ/mol) at  $\sim 1.2$  ML, attributed to the increase in stability with increasing Ca particle size. A 1.0 eV decrease of the work function with Ca coverage from 0 to 0.3 ML indicates that Ca adsorbed at defects is cationic, in agreement with calculations showing that Ca donates electron density to the MgO. Light ion sputtering of the MgO(100) surface generates point defects, but these do not change the heat of adsorption versus coverage, implying that they do not nucleate Ca particles. Oxygen vacancies are a likely candidate; DFT calculations show that F and F<sup>+</sup> center vacancies bind Ca more weakly than terrace sites. More extensive sputtering creates extended defects (such as steps and kinks) that adsorb Ca with heats of adsorption up to  $\sim 400$  kJ/mol, similar to that at the intrinsic defect sites.

### 1. Introduction

The many technologically important applications of metals adsorbed on oxide surfaces, especially in heterogeneous catalysts and microelectronics, photonics and photovoltaic devices, have stimulated vigorous and substantial fundamental research of metal adsorption and film growth on oxide substrates in recent years.<sup>1–6</sup>

The MgO(100) surface is one of the most well-studied oxide surfaces. It has been particularly important in chemisorption studies of small molecules on oxide surfaces,<sup>7–9</sup> as a prototype oxide in studies of metal adsorption, particle nucleation, and growth on oxide surfaces during metal vapor deposition,<sup>10–19</sup> and as the prototypical oxide support in preparing model oxide-

supported transition metal catalysts used to study metal particle size effects in catalysis.<sup>20–23</sup> In such studies, it was often found that adsorption, chemical reaction, and metal particle nucleation occur preferentially at defect sites on MgO(100),<sup>14,15,24–36</sup> as is generally the case for other oxide surfaces as well.<sup>1,37,38</sup>

Alkaline earth metals like Ca are common promoters in solid catalysts,<sup>39–42</sup> where they are often thought to reside on the

<sup>†</sup> University of Washington.

<sup>‡</sup> University of Texas.

- (1) Campbell, C. T. *Surf. Sci. Rep.* **1997**, *27* (1–3), 1–111.
- (2) Campbell, C. T.; Grant, A. W.; Starr, D. E.; Parker, S. C.; Bondzie, V. A. *Top. Catal.* **2001**, *14* (1–4), 43–51.
- (3) Baumer, M.; Freund, H. J. *Prog. Surf. Sci.* **1999**, *61* (7,8), 127–198.
- (4) Wallace, W. T.; Min, B. K. *Top. Catal.* **2005**, *34* (1–4), 17–30.
- (5) Henry, C. R. *Surf. Sci. Rep.* **1998**, *31* (7–8), 235–325.
- (6) St Clair, T. P.; Goodman, D. W. *Top. Catal.* **2000**, *13* (1,2), 5–19.
- (7) Gunster, J.; Liu, G.; Stultz, J.; Krischok, S.; Goodman, D. W. *J. Phys. Chem. B* **2000**, *104* (24), 5738–5743.
- (8) Costa, D.; Chizallet, C.; Ealet, B.; Goniakowski, J.; Finocchi, F. *J. Chem. Phys.* **2006**, *125* (5).
- (9) Pacchioni, G.; Ricart, J. M.; Illas, F. *J. Am. Chem. Soc.* **1994**, *116*, 10152–10158.

- (10) Henry, C. R.; Chapon, C.; Duriez, C.; Giorgio, S. *Surf. Sci.* **1991**, *253* (1–3), 177.
- (11) Pacchioni, G.; Röscher, N. *J. Chem. Phys.* **1996**, *104* (18), 7329.
- (12) López, N.; Illas, F. *J. Phys. Chem. B* **1998**, *102* (8), 1430.
- (13) Musolino, V.; Selloni, A.; Car, R. *J. Chem. Phys.* **1998**, *108* (12), 5044–5054.
- (14) Venables, J. A.; Giordano, L.; Harding, J. H. *J. Phys. Condens. Matter* **2006**, *18* (16), S411.
- (15) Sterrer, M.; Yulikov, M.; Fischbach, E.; Heyde, M.; Rust, H. P.; Pacchioni, G.; Risse, T.; Freund, H. J. *Angew. Chem., Int. Ed.* **2006**, *45* (16), 2630–2632.
- (16) Chiesa, M.; Giamello, E.; Di Valentin, C.; Pacchioni, G.; Sojka, Z.; Van Doorslaer, S. *J. Am. Chem. Soc.* **2005**, *127*, 16935–16944.
- (17) Renaud, G.; Lazzari, R.; Revenant, C.; Barbier, A.; Noblet, M.; Ulrich, O.; Leroy, F.; Jupille, J.; Borensztein, Y.; Henry, C. R.; Deville, J. P.; Scheurer, F.; Mane-Mane, J.; Fruchart, O. *Science* **2003**, *300* (5624), 1416–1419.
- (18) Campbell, C. T.; Starr, D. E. *J. Am. Chem. Soc.* **2002**, *124* (31), 9212–9218.
- (19) Didier, F.; Jupille, J. *Surf. Sci.* **1994**, *309*, 587–590.
- (20) Freund, H. J. *Catal. Today* **2006**, *117* (1–3), 6–14.
- (21) Abbet, S.; Ferrari, A. M.; Giordano, L.; Pacchioni, G.; Hakkinen, H.; Landman, U.; Heiz, U. *Surf. Sci.* **2002**, *514* (1–3), 249–255.
- (22) Becker, C.; Henry, C. R. *Surf. Sci.* **1996**, *352*, 457–462.
- (23) Arenz, M.; Landman, U.; Heiz, U. *ChemPhysChem* **2006**, *7* (9), 1871.

surface of the oxide supports. They are also used as additives to facilitate charge injection at conductive oxide/organic semiconductor interfaces in organic light-emitting devices and photovoltaics.<sup>43,44</sup> Fundamental studies of the interactions of alkaline earth metals with well-defined oxide surfaces have been rather rare, compared to late transition metals.

Here we study the interaction of Ca with MgO(100) and ion-sputtered MgO(100). It is found that Ca binds much more strongly to the extended defect sites on this surface than was reported for late transition metals and lead,<sup>18</sup> although like the late transition metals and lead, Ca atoms bind only weakly and transiently to MgO(100) terraces, where it diffuses rapidly to the defect sites, later to form 3D metal particles. The strong binding of Ca atoms to extended defect sites allows it to be used to interrogate the nature of metal bonding at step sites on MgO(100) surfaces. Since F centers at the step sites on MgO(100) are one of the only (if not the only) defect site on any single-crystal oxide that has also been well characterized by electron paramagnetic resonance and scanning tunneling microscopy (as well as a variety of other spectroscopies),<sup>45</sup> the present results contribute qualitative new information to improve our understanding of the reactivity of these well-defined defect sites. We also find that Ca binds weakly to oxygen vacancies both on the MgO(100) terraces and at step sites, unless the vacancies are charged (F<sup>++</sup> centers). To our knowledge, this is the only report of the experimentally measured adsorption energy of any metal on any defect sites on any oxide surface, although much theoretical effort has been devoted to this recently.<sup>12,13,34,46–48</sup>

## 2. Experimental

The single-crystal adsorption microcalorimetry apparatus and experiments have been described in detail previously.<sup>49</sup> Briefly, the calorimeter is housed in an ultrahigh vacuum chamber, with a base pressure of  $\sim 2$

$\times 10^{-10}$  mbar (rising to  $1 \times 10^{-9}$  mbar, mainly H<sub>2</sub>, during Ca deposition). It is equipped with low-energy electron diffraction (LEED), Auger electron spectroscopy (AES), ion scattering spectroscopy (ISS), a quadrupole mass spectrometer (QMS), a quartz crystal microbalance (QCM), and an ion sputtering gun (LK Technologies).

The calorimeter uses a pulsed metal atom beam and a pyroelectric polymer (PVDF) ribbon pressed against the back of the single crystal to detect the transient temperature rise originating from the adsorption of each gas pulse, as described elsewhere.<sup>49</sup> Different from this previous calorimeter, here we used a so-called double PVDF ribbon assembly, whereby a back ribbon of opposite polarity was placed against the front ribbon to serve as a reference signal which is subtracted from the signal on the ribbon contacting the sample. This eliminates some of the noise signal that originates from the ribbons piezoelectric response to mechanical vibrations, similar to the double ribbon assembly as described previously,<sup>50</sup> but without the Kapton ribbon between the PVDF ribbons. The voltage output (heat signal) is calibrated by using light pulses of known energy as described previously.<sup>49</sup> The typical calorimeter sensitivity was 120–160 V/J (volts at peak maximum per adsorbed joule in the pulse) for these experiments. This is higher than any previous value (typically 10–100 V/J),<sup>49</sup> which we attribute to the better thermal/mechanical contact between the detector and the sample because of the additional force provided by the back ribbon.

A 4-mm diameter, chopped metal atom beam is produced from a high-temperature effusion cell, as described previously.<sup>49</sup> The metal atom beam is chopped to provide 100 ms pulses containing 0.01–0.015 ML Ca every 2 seconds. One monolayer (ML) of Ca is defined throughout as  $1.12 \times 10^{15}$  atoms/cm<sup>2</sup>, which is the MgO(100) unit cell density. The absolute beam flux is measured by using a calibrated quartz crystal microbalance (QCM). The sticking probability is measured by a modified King–Wells method, using a line-of-sight quadrupole mass spectrometer (QMS) at the magic angle<sup>51,52</sup> to measure the fraction of metal atoms which strike the surface but do not adsorb. The mass spectrometer signal is calibrated by measuring the integrated desorption signal for a known amount of multilayer Ca on a Ta foil, located at the same position as the sample, corrected for average velocity.<sup>52</sup>

The typical operating temperature of the effusion cell is  $\sim 1000$  K, which generates some thermal radiation that impinges on the sample and also is detected by the calorimeter (0.07  $\mu$ J/pulse, or  $72.8 \pm 0.4$  kJ of absorbed radiation per mole of dosed Ca). This radiation was measured by blocking the metal beam with a BaF<sub>2</sub> window, which blocks the metal atoms from impinging onto the surface of the sample but passes a known fraction of the radiation. This radiation contribution is subtracted from the total measured signal. The radiation contribution can change if the sample reflectivity changes due to adsorption. We measured the sample reflectivity as described in ref 53. In the coverage range of interest (0–5 ML of Ca), the reflectivity remained constant at 57% with 3% variation.

To convert these measured internal energy changes into standard enthalpy changes at the sample temperature (300 K), the excess translational energy of the metal gas atoms at the oven temperature, above that for a 300 K Maxwell–Boltzmann distribution ( $\sim 0.05$   $\mu$ J/pulse), is subtracted, and a small pressure–volume work term ( $RT$  per mole) is added, as described elsewhere.<sup>49</sup> The corrected enthalpy of

(24) Stirniman, M. J.; Huang, C.; Smith, R. S.; Joyce, S. A.; Kay, B. D. *J. Chem. Phys.* **1996**, *105* (3), 1295–1298.  
 (25) Wang, Y.; Florez, E.; Mondragon, F.; Truong, T. N. *Surf. Sci.* **2006**, *600* (9), 1703–1713.  
 (26) Sanchez, A.; Abbet, S.; Heiz, U.; Schneider, W. D.; Hakkinen, H.; Barnett, R. N.; Landmann, U. *J. Phys. Chem. A* **1999**, *103*, 9573–9578.  
 (27) Abbet, S.; Sanchez, A.; Heiz, U.; Schneider, W. D.; Ferrari, A. M.; Pacchioni, G.; Rösch, N. *J. Am. Chem. Soc.* **2000**, *122* (14), 3453–3457.  
 (28) Xu, L.; Henkelman, G.; Campbell, C. T.; Jonsson, H. *Phys. Rev. Lett.* **2005**, *95* (14), 146103.  
 (29) Bogicevic, A.; Jennison, D. R. *Surf. Sci.* **2002**, *515* (2,3), L481–L486.  
 (30) Fuks, D.; Zhukovskii, Y. F.; Kotomin, E. A.; Ellis, D. E. *Surf. Sci.* **2006**, *600* (9), L99–L104.  
 (31) Matveev, A. V.; Neyman, K. M.; Yudanov, I. V.; Rosch, N. *Surf. Sci.* **1999**, *426*, 123.  
 (32) Xu, L.; Henkelman, G.; Campbell, C. T.; Jonsson, H. *Surf. Sci.* **2006**, *600* (6), 1351–1362.  
 (33) Kim, Y. D.; Stultz, J.; Wei, T.; Goodman, D. W. *J. Phys. Chem. B* **2002**, *106* (27), 6827–6830.  
 (34) Giordano, L.; Di Valentin, C.; Goniakowski, J.; *Phys. Rev. Lett.* **2004**, *92* (9), 096105.  
 (35) Pacchioni, G.; Ferrari, A. M.; *Chem. Phys. Lett.* **1996**, *255* (1–3), 58–64.  
 (36) Scamehorn, C. A.; Harrison, N. M.; McCarthy, M. I. *J. Chem. Phys.* **1994**, *101* (2), 1547–1554.  
 (37) Baumer, M.; Frank, M.; Heemeier, M.; Kuhnemuth, R.; Stempel, S.; Freund, H. J. *Surf. Sci.* **2000**, *454*, 957–962.  
 (38) Min, B. K.; Wallace, W. T.; Goodman, D. W. *J. Phys. Chem. B* **2004**, *108* (38), 14609–14615.  
 (39) Chen, I.; Chen, F. L. *Ind. Eng. Chem. Res.* **1990**, *29*, 534–539.  
 (40) Wu, J.; Shen, Y. M.; Liu, C. H.; Wang, H. B.; Geng, C. J.; Zhang, Z. X. *Catal. Commun.* **2005**, *6* (9), 633.  
 (41) Hou, Z. Y.; Osamu Yokota, O.; Takumi Tanaka, T.; Yashima, T. *Appl. Catal., A* **2003**, *253* (2), 381.  
 (42) Kim, J. S.; Woo, S. I. *Appl. Catal., A* **1994**, *110* (2), 173.  
 (43) Braun, D.; Heeger, A. J. *Appl. Phys. Lett.* **1991**, *58*, 1982.  
 (44) Gustafsson, G.; Cao, Y.; Treacy, G. M.; Klavetter, F.; Colaneri, N.; Heeger, A. J. *Nature* **1992**, *357*, 477.  
 (45) Sterr, M.; Fischbach, E.; Risse, T.; Freund, H.-J. *Phys. Rev. Lett.* **2005**, *94*, 186101.

(46) Del Vitto, A.; Pacchioni, G.; Delbecq, F. O.; Sautet, P. *J. Phys. Chem. B* **2005**, *109* (16), 8040–8048.  
 (47) Giordano, L.; Goniakowski, J.; Pacchioni, G. *Phys. Rev. B* **2001**, *64* (7), No. 075417.  
 (48) Neyman, K. M.; Inntam, C.; Matveev, A. V.; Nasluzov, V. A.; Rosch, N. *J. Am. Chem. Soc.* **2005**, *127* (33), 11652–11660.  
 (49) Stuckless, J. T.; Frei, N. A.; Campbell, C. T. *Rev. Sci. Instrum.* **1998**, *69* (6), 2427–2438.  
 (50) Diaz, S. F.; Zhu, J. F.; Shamir, N.; Campbell, C. T. *Sens. Actuators, B* **2005**, *107* (1), 454–460.  
 (51) Pauls, S. W.; Campbell, C. T. *Surf. Sci.* **1990**, *226* (3), 250–256.  
 (52) Zhu, J. F.; Goetsch, P.; Ruzyczki, N.; Campbell, C. T. *J. Am. Chem. Soc.* **2007**, *129*, 6432–6441.  
 (53) Starr, D. E.; Bald, D. J.; Musgrove, J. E.; Ranney, J. T.; Campbell, C. T. *J. Chem. Phys.* **2001**, *114* (8), 3752–3764.

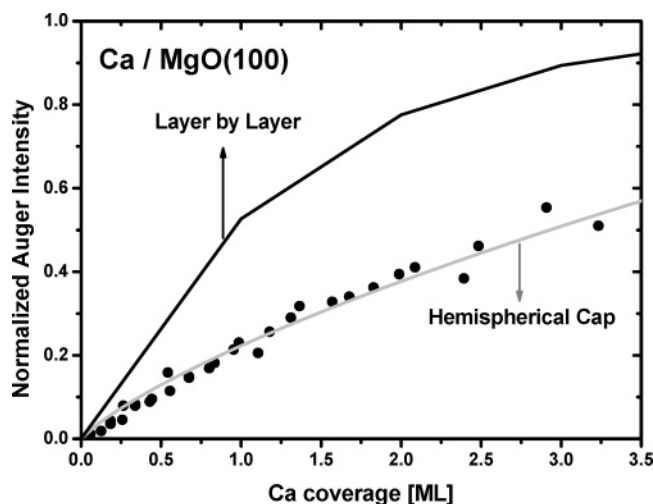


**Figure 1.** The peak-to-peak Ca AES intensity normalized to that of bulk Ca versus coverage for the room-temperature growth of Ca on a thin MgO(100) film grown on Mo(100). The solid curves correspond to what is expected if the Ca film grows in a layer-by-layer growth mode or a hemispherical cap growth model with  $1 \times 10^{12}$  islands/cm<sup>2</sup>, as labeled. The time-averaged Ca flux is nearly the same as in Figure 4, but here it is continuous, not pulsed. The inelastic mean free path used for calculating the two solid curves is 0.93 nm, obtained from the universal curve in ref 59.

adsorption is thus the standard molar enthalpy of adsorption at 300 K, which at high coverage, where the atoms are adding to bulk-like sites, can be compared directly to the standard heat of sublimation of the metal. The measured heats are expressed as the energy of adsorption on a “per mole adsorbed” by correcting for the sticking probability.<sup>49</sup>

The preparation and characterization of the 1  $\mu\text{m}$ -thick Mo(100) single-crystal sample and the  $\sim 4$  nm thick MgO(100) film are described elsewhere.<sup>54</sup>

ISS experiments were carried out using He<sup>+</sup> ions with 1 keV primary energy, as described previously.<sup>52</sup>

Work-function changes ( $\Delta\Phi$ ) were measured by the shifts in the low-energy onset of the secondary electrons in the Auger spectra with the sample negatively biased at 10.00 V, using a very low pass energy ( $\Delta E = 3$  eV) for high resolution and very low electron beam current.

### 3. Results and Discussion

**3.1. Sticking Probability.** We measured the sticking probability of Ca on MgO(100) at room temperature by monitoring the mass spectrometer signal for Ca atoms scattered from the surface. The absence of the detectable Ca signal in mass spectrometry during Ca adsorption up to a coverage of 3 ML indicates that  $<0.5\%$  of the Ca atoms reflect from the surface. Thus, the sticking probability of Ca on MgO(100) is 1.00 over the entire coverage region. This is in contrast to the results of other metals on MgO(100), where the initial sticking probability was 0.7 for Pb,<sup>53</sup> 0.94 for Ag,<sup>54</sup> and 0.995 for Cu,<sup>55</sup> suggesting that Ca interacts more strongly with MgO(100) than these metals, which is also confirmed by the measured heats of adsorption (see below).

**3.2. Growth Mode.** Figure 1 shows the AES results for growth of Ca on the MgO(100) surface at 300 K. The points represent the intensities of the Ca LMM Auger peak at 298 eV normalized to the signal from a thick, bulk-like Ca film on MgO-

(100) ( $>25$  ML) as a function of Ca coverage at 300 K. As can be seen, the intensity of the Ca peak increases continuously with the Ca coverage without any distinct breaks.

The absence of breaks in the Ca AES signal as a function of Ca coverage implies that the growth of Ca on MgO(100) follows the Volmer–Weber (VW, or 3D particle) growth mode.<sup>56</sup> To verify this, we calculated the expected results for both a layer-by-layer growth model<sup>57</sup> and a simple VW hemispherical cap model assuming a constant island density.<sup>58</sup> Those models give the following intensity ratios, respectively:

$$\frac{I_{\text{Ca}}}{I_{\text{Ca}(\infty)}} = 1 - \exp(-d/\lambda_{\text{Ca}} \cos \theta) \quad (1)$$

$$\frac{I_{\text{Ca}}}{I_{\text{Ca}(\infty)}} = nR^2\pi - 2\pi n\lambda_{\text{Ca}}^2 \cos^2 \theta \left[ 1 - \left( 1 + \frac{R}{\lambda_{\text{Ca}} \cos \theta} \right) \exp(-R/\lambda_{\text{Ca}} \cos \theta) \right] \quad (2)$$

where  $I_{\text{Ca}}$  is the Ca AES intensity and  $I_{\text{Ca}(\infty)}$  is the Ca AES intensity from a thick bulk-like Ca layer,  $\lambda_{\text{Ca}}$  is the mean free path of the Ca Auger electrons,  $d$  is the film thickness,  $\theta$  is the detection angle from the surface normal ( $\theta = 45^\circ$  in our case), and  $R$  and  $n$  are the radius and the number density of the hemispherical Ca particles, respectively. Here, we assume this number density is independent of coverage and treat it as a fitting parameter. At any given Ca coverage (total volume), the radius (particle volume) is set by this density. We used the empirical relation obtained by Seah and Dench<sup>59</sup> for 298 eV to get  $\lambda_{\text{Ca}} = 0.93$  nm.

As seen in Figure 1, it is clear that the Ca AES signal falls well below that expected for the layer-by-layer model. Instead, the data coincides very well with the best-fit hemispherical cap model (which assumes an island density of  $1.0 \times 10^{12}$  cm<sup>-2</sup>), suggesting that Ca grows as 3D islands on the MgO(100) surface. The radius of the Ca particles increases to 4 nm at 3 ML coverage in this model. We show below that the saturation population of defect sites is so low (0.06 ML) that it does not affect the AES signal significantly, so it is neglected in this model.

Better evidence of the growth mode is provided by He<sup>+</sup> ion scattering spectroscopy (ISS), since it is more surface sensitive.<sup>60</sup> Figure 2 shows the variations of the integrated Mg and Ca ISS intensities, normalized to those of spectra from the clean MgO(100) surface and the thick Ca overlayer ( $>25$  ML), respectively, as a function of Ca coverage. To verify the negligible effect of He<sup>+</sup>-beam damage to the MgO(100) surface, we did two individual experimental runs with  $\sim$ five-fold different coverage increment size for comparison. The data shown in Figure 2 is a combination of these two individual experimental runs. These two data sets coincided very well, suggesting that beam damage effects are negligible within the accuracy of the ISS experiments. As can be seen, the ISS intensity for Ca increases much more slowly and that for Mg decreases much more slowly with Ca coverage than expected for layer-by-layer growth, strongly

(56) Argile, C.; Rhead, G. E. *Surf. Sci. Rep.* **1989**, *10*, 277–356.

(57) Memeo, R.; Ciccacci, F.; Mariani, C.; Ossicini, S. *Thin Solid Films* **1983**, *109* (2), 159–167.

(58) Diebold, U.; Pan, J.-M.; Madey, T. E. *Phys. Rev. B* **1993**, *47* (7), 3868–3876.

(59) Seah, M. P.; Dench, W. A. *Surf. Interface Anal.* **1979**, *1*, 2.

(60) Ernst, K. H.; Ludviksson, A.; Zhang, R.; Yoshihara, J.; Campbell, C. T. *Phys. Rev. B* **1993**, *47* (20), 13782–13796.

(54) Larsen, J. H.; Ranney, J. T.; Starr, D. E.; Musgrove, J. E.; Campbell, C. T. *Phys. Rev. B* **2001**, *19*, 6319.

(55) Ranney, J. T.; Starr, D. E.; Musgrove, J. E.; Bald, D. J.; Campbell, C. T. *Faraday Discuss.* **1999**, *114*, 195–208.

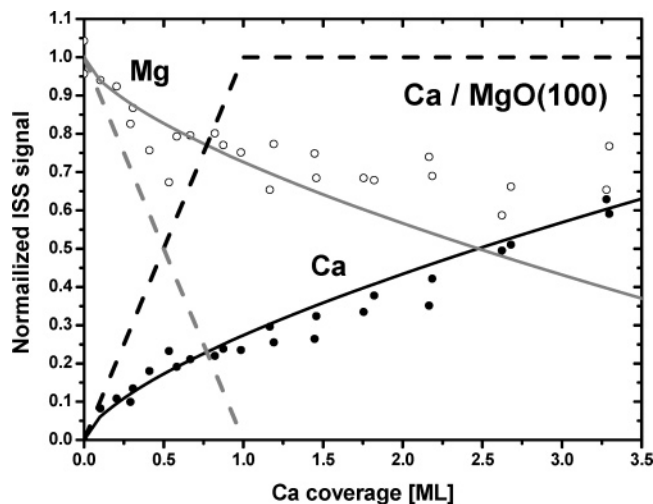


**Figure 2.** Evolution of the normalized Mg (o) and Ca (●) ISS intensities as a function of Ca coverage on a thin MgO(100) film grown on Mo(100) at room temperature. The two solid curves are the calculated ISS results using the island density and radius from the hemispherical cap model's fit to the AES results. The dashed curves show the results expected for layer-by-layer growth.

supporting the VW (3D island) growth mode. Using the hemispherical radius and island density derived from the hemispherical cap fit to the AES results above, we calculated the ISS intensities expected for both Mg and Ca as a function of Ca coverage, assuming that the ISS signal is only from the topmost atomic layer and the neutralization probability of He<sup>+</sup> ions remains constant with Ca coverage. That is, the Ca signal was assumed to be proportional to the projected area of the Ca islands, and the Mg signal proportional to the MgO surface area that is free of Ca. Any shadowing of the Ca-free MgO areas by the Ca hemispheres was neglected. As shown in Figure 2, the calculated Ca ISS signal versus Ca coverage within this model fits the experimental results very well up to ~3.5 ML. While the calculated Mg ISS signal also shows a good fit to the data up to ~1.5 ML, it underestimates the signal somewhat at higher coverages.

LEED measurements were also consistent with Ca growing on MgO(100) as 3D particles. As the Ca coverage increased, the (1 × 1) pattern from the substrate became diffuse and the background intensity increased. No extra spots were observed at any coverage up to 10 ML, suggesting that no ordered Ca overlayer or Ca-induced reconstruction formed uniformly across the surface.

**3.3. Work Function Measurements.** We measured the work function of our clean MgO(100) thin films to be 0.5 ± 0.1 eV below that for the starting clean Mo(100), which has a work function of ~4.4 eV according to the literature (4.53 eV, ref 61; 4.3 eV, ref 62). This sets the work function of our MgO(100) films at ~3.9 eV. Goodman's group reported a work function of 3.25 eV for a similar MgO(100) film on Mo(100),<sup>63</sup> although that same paper also shows that it had the same work function as a multilayer film of benzene grown on it at 100 K, and reports that multilayer benzene on the MgO-free Mo(100) substrate had a work function of 3.9 eV, quite close to our

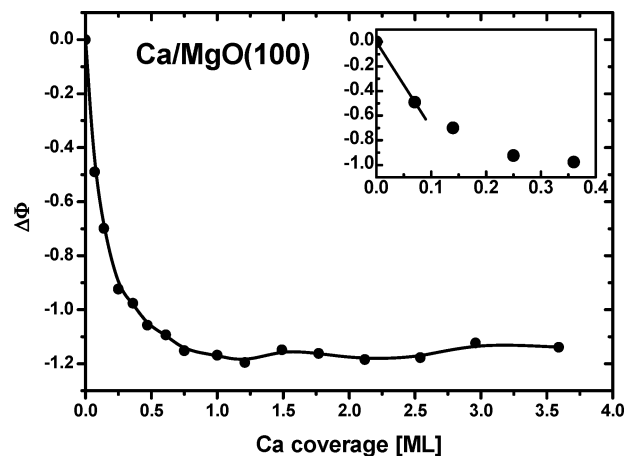


**Figure 3.** Change of the work function versus Ca coverage on MgO(100). Inset: magnified plot of the low-coverage regime.

present result. Still another paper from the same group reports the work function of these MgO(100) films to be 2.7 eV.<sup>64</sup> Charging may cause difficulty in reproducing more exactly the work functions of these insulating MgO (and multilayer benzene) films. Theoretical calculations gave a much larger work function decrease for MgO/Mo(100) (2.1 eV)<sup>65</sup> than we observe (0.5 eV). This may be related to the much thinner MgO films used in those calculations (up to 2–5 layers), compared to the ~20-layer-thick films discussed above.

Figure 3 shows the changes of the work function of the MgO(100) surface as a function of Ca coverage. This curve is an average of four individual experimental results. The work function decreases very sharply with Ca coverage below 0.25 ML, followed by a slower decrease up to ~0.9 ML, after which it remains relatively constant at a value of 1.1 eV below the value of clean MgO(100). This final work function of ~2.8 eV is close to the reported work function of bulk Ca, which is 2.87 eV.<sup>66</sup>

The sharp work function decrease at very low coverages is indicative of a large transfer of electron density from calcium to the MgO substrate or at least a strong polarization of the Ca adatom in that direction, at this initial stage of Ca deposition, where adsorption calorimetry shows that Ca is populating mainly defect sites (see below). The initial slope (<0.1 ML) equals -7 eV/ML, as indicated by the solid line in the inset of Figure 3. Using the Helmholtz equation,<sup>67</sup> the initial slope can be used to calculate the average effective dipole moment of the Ca adsorbate/surface complex at defects:

$$\bar{\mu} = \frac{\epsilon_0 |\Delta\Phi|}{\sigma} \quad (3)$$

Here,  $\bar{\mu}$  is the average effective dipole moment (Debye),  $|\Delta\Phi|$  is the absolute value of work function change slope (eV/ML),  $\epsilon_0$  is the electric vacuum permittivity (Debye·eV<sup>-1</sup>·cm<sup>-2</sup>),  $\sigma$  is the adsorbate concentration (cm<sup>-2</sup>/ML). Using  $|\Delta\Phi| = -7$  eV/ML,  $\epsilon_0 = 2.655 \times 10^{14}$  Debye·eV<sup>-1</sup>·cm<sup>-2</sup>, and  $\sigma = 1.12 \times 10^{15}$  cm<sup>-2</sup>/ML, the average dipole moment of Ca on MgO(100)

(61) Berge, S.; Gartland, P. O.; Slagsvold, B. *J. Surf. Sci.* **1974**, *43*, 275.

(62) Nakane, H.; Satoh, S.; Adachi, H. *J. Vac. Sci. Technol., B* **2005**, *23* (2), 769.

(63) Günster, J.; Liu, G.; Kempter, V.; Goodman, D. W. *Surf. Sci.* **1998**, *415*, 303–311.

(64) Kantorovich, L. N.; Shluger, A. L.; Sushko, P. V.; Günster, J.; Stracke, P.; Goodman, D. W.; Kempter, V. *Faraday Discuss.* **1999**, *119*, 173–194.

(65) Giordano, L.; Cinquini, F.; Pacchioni, G. *Phys. Rev., B* **2006**, *73*, 045414.

(66) Michaelson, H. B. *J. Appl. Phys.* **1977**, *48*, 4729.

(67) Somorjai, G. A. *Introduction to Surface Chemistry and Catalysis*; Wiley: New York, 1994; p 371.

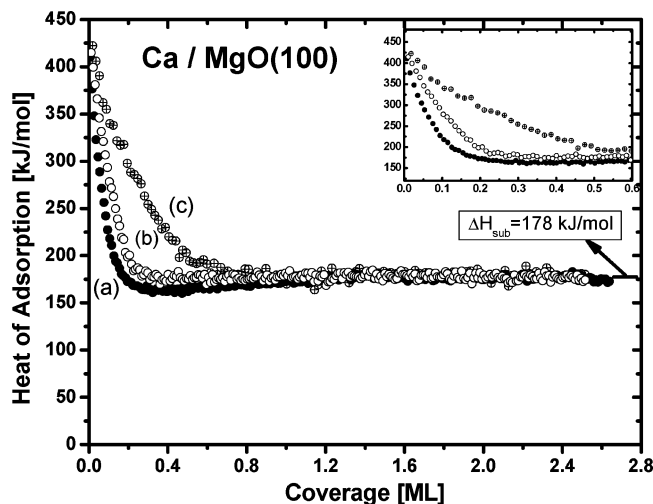


**Figure 4.** The heat of adsorption versus Ca coverage at 300 K for Ca adsorption on (a) a pristine thin MgO(100) film; (b) a thin MgO(100) film irradiated with  $3 \times 10^{14}$  ions/cm<sup>2</sup>; and (c) a thin MgO(100) film irradiated with  $1 \times 10^{16}$  ions/cm<sup>2</sup>. Each data point is due to a pulse of 0.01–0.015 ML of Ca (pulsed at 1/2 Hz) and is the average of three experimental trials, with 1 ML =  $1.12 \times 10^{15}$  atoms/cm<sup>2</sup>, the MgO(100) unit cell density. The inset shows the heats in the low-coverage region (0–0.6 ML) in more detail.

at low coverage is calculated to be 1.7 Debye. This value is much smaller than that of CaO gas molecule (8 Debye<sup>68</sup>), suggesting that only partial charge transfer from Ca to MgO or strong polarization takes place.

Above 1 ML, the work function remains nearly constant at a value near that of solid Ca, although a large but decreasing fraction of the exposed surface area is still MgO, according to ISS. (The remainder is increasingly covered by 3D Ca particles.) Since the work function of an island-covered substrate should be the geometric average of the work functions of the material in the islands and that of the substrate, this suggests that the MgO patches have a lower work function than the starting MgO(100) film, now near that of solid Ca. This is attributed to the population of defects in these MgO areas with Ca<sup>δ+</sup>, which lowers their work function (see above). It is interesting that this saturates at the work function of Ca, which may be associated with electrostatic equilibration. That is, Ca metal can only donate enough charge to lower the MgO work function to that of itself, but no further.

**3.4. Heats of Adsorption: Ca on Pristine MgO(100).** Figure 4 presents the differential heat of adsorption of Ca on MgO(100) at 300 K as a function of Ca coverage. The inset shows the low coverage region (0–0.6 ML) in more detail. The data shown here is an average of three individual experimental runs. The pulse-to-pulse standard deviation (at high coverage where the heats are coverage-independent) is less than 2 kJ/mol for the pulse size used here (only 0.006 ML per pulse), and the run-to-run standard deviation is within 5 kJ/mol. To rule out possible effects on the heats of adsorption of surface damage by electrons while doing AES after the MgO(100) film growth, a calorimetric control experiment of Ca adsorption on MgO(100) was performed, with the surface prepared in exactly the same way but without doing AES or LEED. No significant difference was observed in the initial heat or the heat change versus the coverage.

On the pristine MgO(100) surface, the heat of adsorption starts at 410 kJ/mol (Figure 4, curve a) for the first 0.006 ML adsorbed. It drops very quickly to 210 kJ/mol as the coverage increases to 0.1 ML, followed by a slower decrease to 162 kJ/mol by 0.3 ML. Thereafter it increases slightly to a nearly constant value of 178 kJ/mol by 1.2 ML, corresponding excellently with the bulk heat of sublimation of Ca ( $\Delta H_{\text{sub}} = 177.8$  kJ/mol<sup>69</sup>). The initially high heat of adsorption and its rapid decrease to a minimum will be attributed to the saturation of intrinsic defect sites on the surface (see below). The small rise in heat beyond this minimum occurs in a coverage range where Ca is mainly populating 3D Ca particles. We interpret this as being due to the effect of particle size on the energy of metal nanoparticles, similar to that we have reported previously for Pb and Ag adsorption energies on nanoparticles on MgO(100).<sup>18,70</sup> The fact that this increase stops at a stable value after 1.2 ML indicates that, by 1.2 ML, Ca is adding mainly to pure bulk-like 3D Ca particles that are large enough to not change in adsorption energy significantly with increasing size. At this coverage, the Ca particles are  $\sim 2.2$  nm in radius according to the hemispherical cap model used to fit the AES data above. Similarly for Pb adsorbing onto Pb nanoparticles on MgO(100), the heat of adsorption increase with Pb particle size occurs mainly below  $\sim 2.5$  nm radius.<sup>70</sup>

The initial heat of adsorption is much higher than the heat of sublimation of bulk Ca, indicating that the Ca atoms bond very strongly to the MgO(100) surface initially. However, the sharp decrease in the heats from 410 to 210 kJ/mol within 0.1 ML suggests that only a very small amount of the MgO(100) sites adsorb Ca strongly, which is also consistent with the above work function measurements. This small amount suggests some sort of intrinsic surface defect sites on the MgO surface.

**3.5. Heats of Adsorption: Ca on Ar<sup>+</sup> Sputtered MgO(100).** Often, the point defects on MgO(100) surfaces, including O vacancies on terraces (which can be F, F<sup>+</sup>, or F<sup>2+</sup> centers depending on their charge), Mg vacancies (V, V<sup>-</sup>, or V<sup>2-</sup> centers) and divacancies (missing Mg–O pairs), play an important role in the nucleation of metal particles, particularly for transition and noble metals.<sup>15,29–33</sup> Oxygen vacancies in the terraces are the most common point defect, although their density should be small for our sample preparation<sup>45,71</sup> and thus unlikely to affect the results in Figures 1–4a. Recent results show that they are much more likely to be present along step edges<sup>3,45,72,73</sup>

To investigate the effects of surface point defects on the adsorption energies of Ca, we created these defects by lightly sputtering the pristine MgO(100) surface at 300 K with Ar<sup>+</sup> ions (1000 eV). Surprisingly, ion doses below  $10^{14}$  ions/cm<sup>2</sup> caused no significant change in the heat of Ca adsorption versus coverage. This implies that the point defects created in this way (oxygen vacancies<sup>74</sup>) bind Ca atoms more weakly than small 3D Ca particles (that is,  $< 162$  kJ/mol, see above).

(68) Sakamoto, S.; White, G. J.; Kawaguchi, K.; Ohishi, M.; Usuda, K. S.; Hasegawa, T. *Mon. Not. R. Astron. Soc.* **1998**, *301*, 872.

(69) Lide, D. R. *CRC Handbook of Chemistry and Physics*, 87th ed.; CRC Press: Boca Raton, FL, 2006.

(70) Campbell, C. T.; Parker, S. C.; Starr, D. E. *Science* **2002**, *298* (5594), 811–814.

(71) Kim, Y. D.; Stultz, J.; Goodman, D. W. *Surf. Sci.* **2002**, *506* (3), 228–234.

(72) Sterrer, M.; Heyde, M.; Novicki, M.; Nilius, N.; Risse, T.; Rust, H.-P.; Pacchioni, G.; Freund, H.-J. *J. Phys. Chem. B* **2006**, *110*, 46–49.

(73) Carrasco, J.; Lopez, N.; Illas, F.; Freund, H.-J. *J. Chem. Phys.* **2006**, *125*, 074711.

(74) Peterka, D.; Tegenkamp, C.; Schroder, K. M.; Ernst, W.; Pfnur, H. *Surf. Sci.* **1999**, *431* (1–3), 146–155.

Larger doses of the Ar<sup>+</sup> ions ( $3 \times 10^{14}$  ions/cm<sup>2</sup> and  $1 \times 10^{16}$  ion/cm<sup>2</sup>) led to significantly increased heats of adsorption at moderate coverages, as shown in Figure 4. Given that the neutral gas atom sputter yield per Ar<sup>+</sup> ion collision with surfaces at this energy is typically several atoms,<sup>75,76</sup> these ion doses are sufficient to create contiguous or extended defects, and not just point defects. Interestingly, the heats of adsorption for both low ( $3 \times 10^{14}$  ions/cm<sup>2</sup>) and high ( $1 \times 10^{16}$  ions/cm<sup>2</sup>) doses of Ar<sup>+</sup> ions sputtered surfaces start at almost the same value (~400 kJ/mol) as that observed on the pristine MgO(100) surface. Moreover, the heats of adsorption decay more slowly to the heat of bulk Ca sublimation on the sputtered surfaces compared to the pristine surface, and the higher the Ar<sup>+</sup> ion dose is, the slower this decay is. This suggests that these large ion doses create more of the same types of defects which give rise to the high initial heat of adsorption on the pristine surface.

#### 4. Density Functional Theory Calculations

Ab initio calculations have been used to identify the binding sites of Ca on MgO(100) and give a microscopic description of the coverage-dependent adsorption energy measured on the pristine and sputtered surfaces.

Our calculations are based upon density functional theory (DFT) using the PW91 generalized gradient approximation (GGA) functional.<sup>77</sup> Frozen core charges were modeled with pseudopotentials using the projected augmented wave approach as implemented in the VASP code.<sup>78</sup> A plane wave basis set with an energy cutoff of 250 eV (appropriate for the pseudopotentials) described the valence electrons in our periodic supercell, and a  $2 \times 2 \times 1$  Monkhorst-Pack grid<sup>79</sup> was found to be sufficient for sampling the Brillouin zone. Spin-polarized calculations were tested for each binding site and used when necessary. The MgO substrate was modeled with three- or four-layers with at least 36 atoms per layer per supercell. Larger substrates were used to check for system size interactions between adsorbates and defect sites. The lowest two layers were held frozen at the optimal DFT lattice constant of 4.23 Å, which compares favorably to the experimental lattice constant of 4.21 Å. Substrates with a step edge were formed by tilting the surface so that a single step was present in the cell. Geometry optimizations were considered converged when the residual force dropped below 0.001 eV/Å on each atom. For charged cells, a uniform background compensation charge was applied. Additional details of our calculations will be provided in a separate publication.<sup>80</sup>

**4.1. Binding sites of Ca on MgO(100).** The Ca monomer adsorbs directly above an O atom on the MgO(100) terrace with an energy of 0.84 eV (82 kJ/mol), as shown in Figure 5(a and b). A Bader charge density analysis,<sup>81,82</sup> which partitions charge into volumes defined by zero-flux surfaces around each atom, shows a charge transfer of 0.24 e from the Ca atom to the oxide.

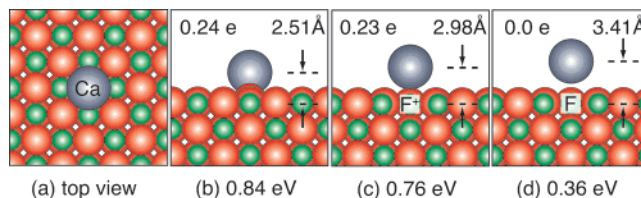


**Figure 5.** According to DFT, Ca binds to the O site on the MgO terrace (b) with 0.84 eV (82 kJ/mol), and less strongly at F<sup>+</sup> and F oxygen vacancies (c and d). This indicates that the heat of adsorption of Ca on MgO will not be significantly affected by these point defects. The amount of charge transfer from Ca to the surface at the different sites correlates with the interaction strength. (Note: O atoms are red, Mg atoms are green, and the Ca atom is gray.)

Only 18% of this charge is transferred to the O atom directly below the adsorbed Ca atom, but the majority (83%) is transferred to that O atom and its (Mg and O) neighbors in the top MgO layer. If we make the assumption that the charge of 0.24 e is transferred from the Ca to the oxide over a distance of 2.51 Å (see Figure 5), we calculate a charge-transfer induced dipole of 2.9 D per adsorbed Ca atom. Furthermore, if we calculate the dipole from a direct integration of the charge difference due to the adsorption of Ca, we find a similar dipole of 3.3 D. This shows that the dipole can be explained by charge redistribution between the Ca atom and the oxide substrate rather than from polarization within the Bader volume around the Ca atom. A dipole of 3.3 D results in an initial decrease of 14 eV/ML in the work function as Ca is adsorbed on MgO—roughly twice what is observed experimentally. An initial binding site with a smaller charge-transfer would be more consistent with the experimental change in work function.

In this discussion, we are using the term charge-transfer somewhat loosely: we are not implying that an electron from the Ca transfers to a state in the oxide. Rather, we are saying that the induced dipole can be accurately calculated from a Bader population analysis, without considering polarization within the Bader volumes. Our description is not necessarily inconsistent with results from Chiesa et al.,<sup>16</sup> which describe the dipole created when K is adsorbed on MgO as being due to the polarization of the K atom. In this calculation a Mulliken population analysis is used, for which charge density in the oxide surface could still be associated with the K atom and not described in terms of charge transfer as in the Bader analysis.

When a Ca adatom lands on the terrace, it can hop between O sites with a barrier of 0.45 eV. At room temperature, this diffusion is rapid so that the Ca adatoms will find and be trapped at stronger binding sites, if present even in very low concentration. It is the binding energy of Ca to these point or extended defects that determines the experiment's initial heat of adsorption, rather than Ca binding to the terraces.

In previous studies of cleaved MgO surfaces, point defects were found to nucleate Pd island growth on the terrace.<sup>83</sup> AFM images of Pd clusters showed that the pinning defects, presumably oxygen vacancies, were present on the surface with a concentration of  $3 \times 10^{12}$  cm<sup>-2</sup>. Later studies on grown MgO surfaces concluded that singly charged (F<sup>+</sup>) oxygen vacancies were not present because there was no significant EPR signal detected on the pristine surface.<sup>45</sup>

(75) Andersen, H. H.; Bay, H. L. *Sputtering by Particle Bombardment*. In *Topics in Applied Physics*; Behrisch, R., Ed.; Springer-Verlag: Berlin, 1981; Vol. 47, p 145.

(76) Ramana Murty, M. V. *Surf. Sci.* **2002**, *500*, 523.

(77) Perdew, J. P. In *Electronic Structure of Solids*; Ziesche, P., Eschrig, H., Eds.; Akademie Verlag: Berlin, 1991.

(78) Kresse, G.; Joubert, J. *Phys. Rev. B* **1999**, *59*, 1758.

(79) Monkhorst, H. J.; Pack, J. D. *Phys. Rev. B* **1976**, *13* (12), 5188–5192.

(80) Xu, L.; Henkelman, G. Unpublished work.

(81) Bader, R. F. W. *Atoms in Molecules: A Quantum Theory*; Oxford University Press: New York, 1990.

(82) Henkelman, G.; Arnaldsson, A.; Jónsson, H. *Comput. Mater. Sci.* **2006**, *36*, 354–360.

(83) Haas, G.; Menck, A.; Brune, H.; Barth, J. V.; Venables, J. A.; Kern, K. *Phys. Rev. B* **2000**, *61*, 11105–11108.

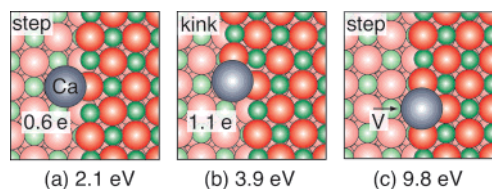


**Figure 6.** DFT calculations show that Ca binds with 2.1 eV (205 kJ/mol) at step sites (a) and 3.9 eV (376 kJ/mol) at kink sites (b). For the experimental deposition temperature, Ca binds irreversibly to these extended defects, so that they will contribute to the measured initial heat of adsorption (410 kJ/mol) in proportion to their relative population. Stronger binding sites, such as Mg vacancies (V-center) in the steps (c) give rise to higher binding energies, 9.8 eV (946 kJ/mol), and would, even in small abundance, bring the calculated (average) initial binding energy up to what is observed.

To determine if deposited Ca atoms are similarly trapped at such point defects and nucleate clusters, we calculated the binding energy of Ca at both neutral (F) and charged (F<sup>+</sup>) oxygen vacancies. Figure 5 parts c and d show that Ca binds more weakly to these defects than to the terrace. An explanation for this can be seen from the Bader charge of the Ca ion. On the terrace and F<sup>+</sup> center a charge of 0.24 and 0.23 e is transferred to the O and F<sup>+</sup> center, respectively. The neutral F center, however, is saturated with electrons from the neighboring Mg ions, and does not accept any additional charge from the Ca. In the case of either defect (F or F<sup>+</sup>) the Ca binds less strongly than on the terrace, so we do not expect these sites to contribute to the heat of adsorption at low coverage, even if they are present on the surface. Ca atoms that reach these sites will continue diffusing until they find stronger-binding sites.

Step and kink sites are expected to be present on the pristine surface. STM images of similarly grown MgO(100) thin films show a high density of such sites.<sup>45,84</sup> Our calculations (see Figure 6) show that a Ca monomer binds to a straight step edge site with an adsorption heat of 2.1 eV (205 kJ/mol) and a charge transfer of 0.6 e. Most of this charge (68%) is transferred to the under-coordinated O atoms in the step and does not contribute to the dipole moment perpendicular to the surface. An integration of the charge difference shows this dipole perpendicular to the surface to be 2.3 D, causing an initial work function drop with slope  $-9.7$  eV/ML, much closer to the experiment ( $-7$  eV/ML) than Ca binding to the terrace ( $-14$  eV/ML). An important point is that Ca binds irreversibly to any site along the step edge. To diffuse along the step, the Ca atom must dissociate from the step onto an O terrace site nearby, overcoming a barrier of 1.4 eV. Thus, at room temperature, Ca atoms that diffuse to step edges bind irreversibly where they initially attach, releasing 2.1 eV, and cannot diffuse along the step edge.

Ca atoms can also bind to kinks and stronger binding sites on the surface. Kink sites are certainly present, and DFT shows that Ca atoms bind strongly to them with an adsorption heat of 3.9 eV (376 kJ/mol). The dipole created by Ca binding at kinks, normal to the surface, is small. There is a significant charge transfer (1.1 e) to the under-coordinated atoms in the step, but the dipole perpendicular to the surface is only 0.09 D. Other possible strong binding sites include Mg vacancies (V centers) or divacancies. Ca binds strongly to these sites by filling the

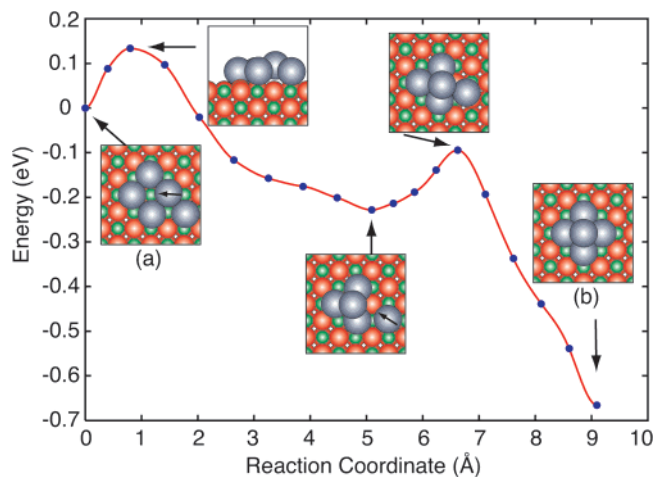


**Figure 7.** According to DFT, a flat Ca pentamer forms a three-dimensional cluster by crossing a barrier (0.13 eV) that is lower than the monomer diffusion barrier (0.45 eV). Clusters of five or more Ca atoms are expected to spontaneously form three-dimensional clusters, which is consistent with the ISS and AES measurements.

Mg vacancy. An example of this is shown in Figure 6c, in which a Ca atom has filled a V center at a step. The binding energy of 9.8 eV is very high at this defect—and at any defect containing an Mg vacancy. We also considered Ca binding to O vacancies at steps, however this is weaker (1.3 eV) than at a regular step site (2.1 eV). F<sup>+</sup> centers at steps bind Ca somewhat stronger (1.9 eV), but since it is still weaker than at the step, neither oxygen vacancy defect is expected to affect the heat of adsorption of Ca.

**4.2. Ca Clusters.** In the initial stages of Ca deposition, Ca monomers diffuse across the terrace until they bind irreversibly at steps, kink, and stronger binding sites. Subsequent monomers will form small Ca clusters at these binding sites. Clusters of two and three Ca atoms sit flat on the MgO(100) terrace. The tetramer is isoenergetic as a two- and three-dimensional cluster, but larger clusters spontaneously form stable three-dimensional clusters. Figure 7 shows a climbing-image nudged elastic band calculation<sup>85,86</sup> starting from a two-dimensional Ca pentamer on a MgO(100) terrace. This calculation shows the minimum energy pathway by which the cluster takes a three-dimensional pyramidal structure, crossing a barrier of only 0.13 eV. Since this barrier is lower than the diffusion barrier of the Ca monomer, and accessible at room temperature, this and larger clusters are expected to assume three-dimensional structures. The cohesive energy of three-dimensional clusters is dominated by Ca–Ca bonds and thus should quickly reach that of bulk Ca as the clusters grow, as seen experimentally.

## 5. Discussion: A Two-State Model

The initial, nearly linear decrease in the heat of adsorption with coverage seen in all the curves of Figure 4 could arise because of a first-order Langmuir-like probability of populating a single type of defect site with a heat of adsorption of 410 kJ/mol, in competition with populating 3D Ca clusters. On the basis of these experiments and our DFT calculations, we propose a simplified two-state growth model to explain the measured heat of adsorption of Ca, whereby all the Ca-trapping defects

(84) Benedetti, S.; Benia, H. M.; Nilius, N.; Valeri, S.; Freund, H. J. *Chem. Phys. Lett.* **2006**, *430*, 330–335.

(85) Henkelman, G.; Jónsson, H. *J. Chem. Phys.* **2000**, *113*, 9978–9985.

(86) Henkelman, G.; Uberuaga, B. P.; Jónsson, H. *J. Chem. Phys.* **2000**, *113*, 9901–9904.

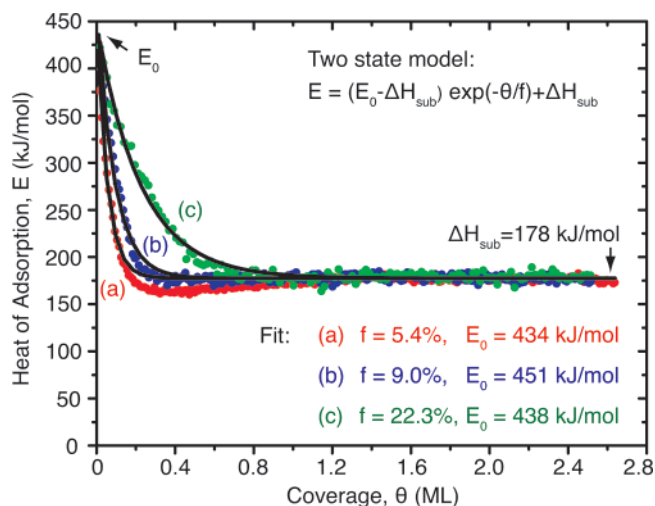


**Figure 8.** The experimental heat of adsorption data fit to a two-state model. On the annealed surface (a) the concentration of defect sites is found to be 5.4%, and their average binding energy is 434 kJ/mol (4.5 eV). For light (b) and heavy (c) sputtered surfaces, the concentration of defect sites increases to 9.0% and 22.3% respectively, but the initial binding energy does not systematically change. This indicates that Ar<sup>+</sup> sputtering creates the same kinds of strong (extended) intrinsic defects that are found on the annealed surface.

types are grouped into a single “average defect” state. Our DFT calculations show that at low coverage Ca monomers initially diffuse rapidly on the terrace at room temperature, repelling oxygen vacancy defects, until they bind irreversibly at strong-binding intrinsic defect sites. Many of these monomers will bind at steps sites (205 kJ/mol), kink sites (376 kJ/mol), and even stronger binding sites such as the Mg vacancy at steps (946 kJ/mol). Since these sites irreversibly trap Ca atoms, the initial heat of adsorption will be an average of these defect binding energies,  $E_i$ , weighted by the relative population of each binding site,  $f_i$ . This initial binding energy,  $E_0$ , can be written as

$$E_0 = \sum_i E_i f_i \quad (4)$$

In our two-state model, we assume that, after such an “average” defect site is occupied by a Ca monomer (giving off an average heat of adsorption of  $E_0$ ), the site becomes a nucleation center for Ca clusters. For simplicity, we further assume that subsequent monomers bind to this site and release the heat of sublimation for bulk Ca,  $\Delta H_{\text{sub}} = 178$  kJ/mol. The heat of adsorption,  $E(\theta)$ , can then be represented by:

$$E(\theta) = (E_0 - \Delta H_{\text{sub}})e^{-\theta/f} + \Delta H_{\text{sub}} \quad (5)$$

where  $\theta$  is the coverage,  $f$  is the fraction of sites on the surface that irreversibly bind a Ca monomer at room temperature (i.e., the defect fraction), and  $E_0$  is the average binding energy of these defect sites for a Ca monomer.

The exponential decay, predicted by this model, is a good fit to the initial decay in the measured heat of adsorption, and the plateau at higher coverage (see Figure 8). The experimental data falls slightly below the model at coverages around  $1/2$  ML. This is because Ca clusters below  $\sim 5$  nm in diameter are expected to have a lower heat of adsorption than the bulk heat of sublimation, as shown for Pb/MgO.<sup>70</sup> (This size effect is not so

dramatic for Ca as it was for Pb, because Ca binds much more strongly to MgO relative to clusters than does Pb.)

The fitting parameters from this two-state model (listed in Figure 8) illustrate some interesting aspects of the data. First, on the pristine surface (a), we find 5.4% defect sites with an average heat of adsorption of 434 kJ/mol. According to DFT, the average heat at step and kink sites is lower than this (205 and 376 kJ/mol, respectively). This implies that either (1) the surface has more defect sites than 5%, (2) these DFT results underestimate the true strength of Ca–defect bonding, and/or (3) there is some other type of defect present (such as Mg vacancies or impurities at step edges), that binds Ca more strongly than steps and kinks and contributes some fraction to the high initial heats. While it would not be surprising if DFT underestimated binding energies by the 58 kJ/mol difference between this value of 434 kJ/mol and the DFT result for kink sites, it is very unlikely that DFT is in error by the 234 kJ/mol difference between this value and DFT result for step sites. While we do not know what fraction of the step sites are kinks, STM images of similar MgO(100) thin films show a lot of curvature along the step edges,<sup>84</sup> consistent with a substantial fraction of kinks.

When Ar<sup>+</sup> is used to sputter the surface, the fraction of defects sites increases to 9.0% with moderate sputtering (Figure 8a) and 22.3% with heavy sputtering (Figure 8b). What is remarkable about the data, however, is that within the uncertainty of our fits, the initial binding energy remains constant with increased sputtering. This indicates that sputtering does not create any new sites that bond Ca adatoms significantly more strongly than the film’s intrinsic surface defect sites. Extended defects (such as steps and kinks) are more stable and evolve with heavy sputtering. It is rather surprising that the initial heat does not change upon sputtering, since this implies within our model (wherein Ca is immobile once trapped at such defects) that the population-weighted average heat of the many different types of defects thus created just happens to match closely that of the as-grown MgO(100) film.

## 6. Conclusions

Calcium adsorbs with unit sticking probability on MgO(100) at 300 K, initially binding at strong binding defect sites (steps, kinks, and possibly even impurities on the step edges) with a very high heat of adsorption ( $\sim 410$  kJ/mol). The heat of adsorption decreases rapidly with coverage as the kinks and steps saturate. The strong decrease in work function with Ca coverage in this range indicates that Ca adatoms at kinks and steps are cationic, and the measured slope of  $-7$  eV/ML is qualitatively consistent with the adsorption-induced dipole from DFT calculations of Ca binding at these sites. The heat reaches a minimum of 162 kJ/mol at  $\sim 0.3$  ML, where Ca is mainly adding to small 3D Ca clusters, with density  $\sim 1 \times 10^{12}$  cm<sup>-2</sup>. Afterward, it increases to the value of bulk Ca’s heat of sublimation (178 kJ/mol) by  $\sim 1.2$  ML, as the Ca particle size increases. DFT calculations show that point defects (probably oxygen vacancies) created by ion sputtering bind Ca more weakly ( $< 80$  kJ/mol) than monomers on the terrace and hence do not change the initial heat of adsorption. Experiments show that the defects created by more extensive sputtering adsorb Ca with heats of adsorption up to  $\sim 420$  kJ/mol, similar to that at the intrinsic strong-binding defects.

**Acknowledgment.** The authors would like to acknowledge the Department of Energy, Office of Basic Energy Sciences, Chemical Sciences Division Grant No. DE-FG02-96ER14630 for support of this work. J.A.F. would like to acknowledge the Center for Nanotechnology at the UW for an NSF-supported IGERT Award (DGE-0504573). G.H. gratefully acknowledges

the National Science Foundation for a CAREER Award (No. CHE-0645497) and the Robert Welch Foundation (No. F-1601). The calculations were carried out on Texas Advanced Computing Center (TACC).

JA077865Y